THE JOURNAL OF PHYSICAL CHEMISTRY A

Article

pubs.acs.org/JPCA

SmB_6^- Cluster Anion: Covalency Involving f Orbitals

Paul J. Robinson,[†] Xinxing Zhang,[‡] Tyrel McQueen,[‡] Kit H. Bowen,*[,‡] and Anastassia N. Alexandrova*[,†,§]

[†]Department of Chemistry and Biochemistry, University of California, Los Angeles, 607 Charles E. Young Drive East, Los Angeles, California 90095, United States

[‡]Department of Chemistry and Materials Science, Johns Hopkins University, 3400 N. Charles Street, Baltimore, Maryland 21218, United States

[§]California NanoSystems Institute, 570 Westwood Plaza, Building 114, Los Angeles, California 90095, United States

ABSTRACT: While boride clusters of alkali and transition metals have been observed and extensively characterized, so far little is known about lanthanide−boron clusters. Lanthanide−boride solids are intriguing, however, and therefore it is of interest to understand the fundamental electronic properties of such systems, also on the subnano scale. We report a joint experimental photoelectron spectroscopic and theoretical study of the SmB_6^- anion, iso-stoichiometric to the SmB_6 solid—a topological Kondo insulator. The cluster is found to feature strong static and dynamic electron correlations and relativistic components, calling for treatment with CASPT2 and up sixth-order Douglass−Kroll−Hess (DKH) relativistic correction. The cluster has a C_{2v} structure and covalent Sm−B bonds facilitated by f atomic orbitals on Sm, which are typically thought to be contracted and inert. Additionally, the cluster retains the double antiaromaticity of the B_6^{2-} cluster.

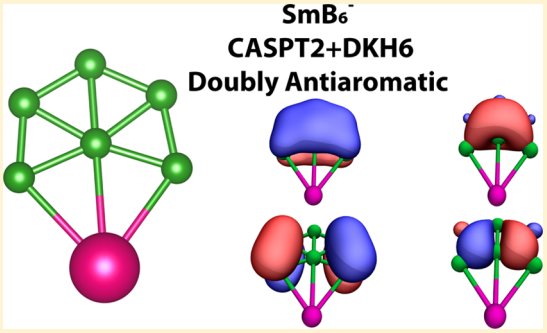

INTRODUCTION

Small boron clusters are fascinating because they possess a multitude of bonding motifs. In the smallest cluster anions ($B_n^{1/2-}$, $n < 40$) we encounter a diverse group of planar and quasi-planar structures, governed by both strong covalent bonds as well as delocalized (anti)aromatic bonding. For example, B_3^- (D_{3h}) and B_4^- (D_{2h}) are doubly and triply aromatic, respectively.[1] Even with large structures like B_{36}^-, highly symmetric and aromatic boron structures are favored.[2] Planarity of these structures is enforced by covalent two center−two electron (2c−2e) B−B bonds, while the delocalized bonding arrangements dictate the symmetry of the planar structures. On the other hand, the all-boron fullerene, named borospherene, B_{40}, possesses not a single 2c−2e B−B bond, and instead, all the bonds in this species are multicenter.[3] This cluster marks a clear difference between the chemistries of boron and its nearest neighbor—carbon. Bulk boron allotropes are three-dimensional and feature a prominent B_{12} icosahedral motif. These boron systems demonstrate the metalloid nature of boron: it will form strong covalent B−B bonds, and also delocalized bonds, of both σ and π types.[4,5]

Boron clusters only become more interesting upon the addition of a metal. The metal-like nature of boron allows for an actual metal to weave into an existing aromatic network, leading to high stability. One exciting example of this is $Co©B_8^-$ (D_{8h}), a wheel structure that is aromatic and can be rationalized with the dual nature of boron—the strong covalent bonds between each boron make the ring stable on the outside, while boron's propensity for delocalized bonding creates an aromatic system containing the central cobalt.[6] This bonding motif is not an exception; in fact, both ruthenium and tantalum were shown to form nearly identical wheels with nine and ten borons, respectively. Lastly, a similar "drum"-looking cluster CoB_{16}^- also shows strong bonds between every two borons, in addition to an overall aromaticity of the system.[7,8] At the same time, small boron clusters were shown to serve as possible ligands to metals.[9] B_8^{2-} and B_6^{2-} both retain their planar structure and aromatic/antiaromatic bonding upon coordination to small cations such as Li^+.[10,11] The boron ligands are anionic in these cases. Thus, boron is promiscuous when binding to metals: it can be covalent or anionic, and this property certainly characteristic of its metalloid nature. Boron is perfectly matched with d-block metals to form dually covalent and aromatic structures, and it is an anion with alkali metals. How would boron behave when coordinating lanthanides, for example samarium?

Lanthanides are large atoms (the Sm atom has a covalent radius of 1.98 Å) as compared to the tiny second-row boron (0.84 Å in the neutral state).[12] This large difference seems to be detrimental to a possible covalent overlap. The possibility of ionic bonding is more plausible due to the difference in electronegativities: 2.04 for B and 1.17 for Sm. Indeed, Sm, along with La and Yb, form solid hexaborides, and SmB_6 in particular is a topological Kondo insulator,[13−15] possessing the

Received: January 9, 2017
Revised: February 8, 2017
Published: February 9, 2017

DOI: 10.1021/acs.jpca.7b00247
J. Phys. Chem. A 2017, 121, 1849−1854

Sm^{2+}/Sm^{3+} mixed valency.[16] In order to eventually understand the bonding in these solids, as well as in general in lanthanide−boron systems, we begin exploration from the SmB_6^- gas phase anion, stoichiometrically identical to the famous SmB_6 solid.

EXPERIMENT

The SmB_6^- cluster ion was obtained in the gas phase, and its photoelectron spectrum was recorded. Anion photoelectron spectroscopy was conducted by crossing a mass-selected beam of negative ions with a fixed-frequency photon beam and energy-analyzing the resultant photodetached electrons. Our anion photoelectron spectrometer, which has been described previously, consists of a laser vaporization anion source, a linear time-of-flight mass analyzer/selector, a pulsed Nd:YAG photodetachment laser, and a magnetic bottle electron energy analyzer.[17,18] Photoelectron spectra were calibrated against the well-known photoelectron spectrum of Cu^-.[19] Parent anions of SmB_6^- were generated in a laser vaporization source. Briefly, a 1/4 in. diameter SmB_6 rod was interrogated by a pulsed Nd:YAG laser beam operating at a wavelength of 532 nm. The resulting plasma was cooled by supersonically expanding a plume of helium gas from a pulsed gas valve (backing pressure of ~150 psi). Negatively charged anions were then extracted into the spectrometer prior to mass selection and photodetachment. The experimental spectrum is shown in Figure 1.

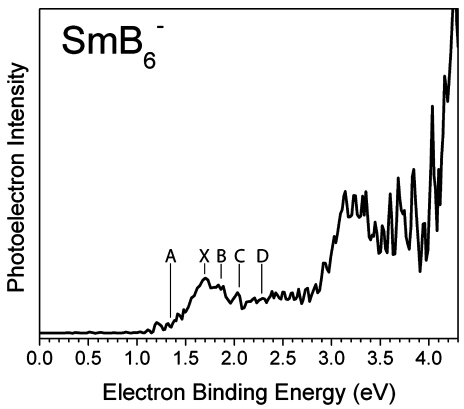

Figure 1. Experimental photoelectron spectrum of SmB_6^-. A, X, B, C, and D denote the transitions from the ground state of the anion to the ground and excited states of the neutral.

THEORY

Because of the diverse nature of previously observed boron clusters, as well as the oft-counterintuitive properties of heavy elements like Sm, we do not lean heavily on our chemical intuition in determining the structure of this boride. In fact, a question we wish to answer is whether samarium and lanthanides in general coordinate to boron similarly to other metals. At the same time, the geometric configuration space is vast enough with seven atoms that a little guiding logic is necessary. In general, boron will create bonds with itself, so we should preference starting seed structures with boron close to itself and in groups.

To find the global minimum of SmB_6^-, we randomly generated about a hundred structures by distributing atoms randomly around the van der Waals radii of the atoms and observed which types of structures were likely to converge single point DFT calculations. The results of this trial informed our starting structure logic and allowed us to save on computation time. Using this, we generated several hundred random structures and selected 40 probable starting structures. We included a few nonprobable structures to minimize our chances of missing a minimum. Each structure was geometry optimized to the nearest minimum at the PBE0+ZORA level of theory with the all-electron SARC-ZORA basis set on Sm and the 6-31+G* basis on B.[20−22] PBE0 was chosen because it is known to work well for predicting geometries. All the calculations for the optimization were run using NWChem 6.5.[23] We optimized each starting structure in four multiplicities: quartet, sextet, octet, and decet. We also took each converged minimum and ran a geometry optimization of the converged structure in the other multiplets. The lowest 26 minima are shown in Figure 2.

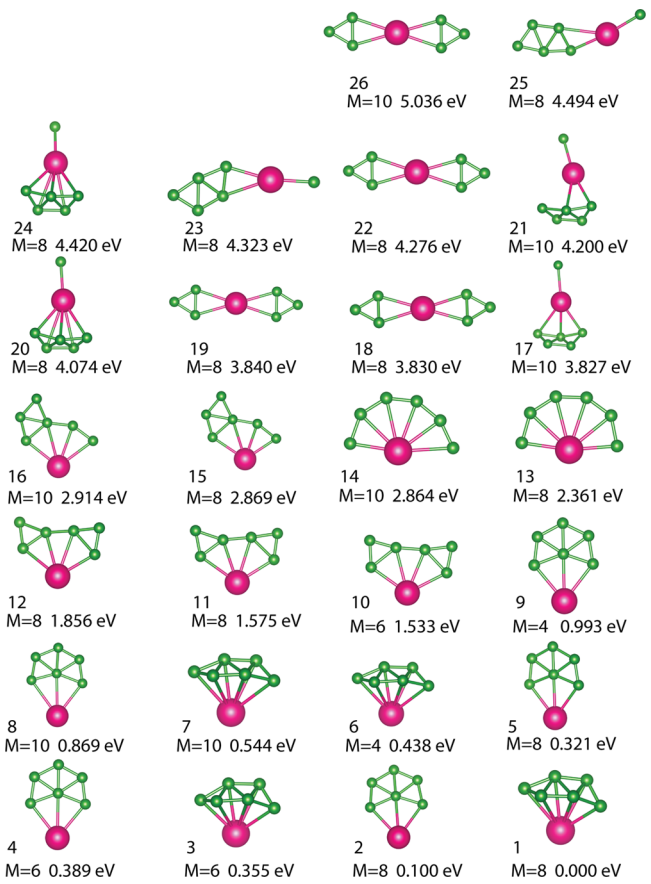

Figure 2. Low-lying minima from a PBE0 global geometry optimization of SmB_6^-. The energies shown are relative to the lowest energy structure. *M* denotes the multiplicity. Because only 0.1 eV separates our lowest two minima, it is necessary to approach this system with higher levels of theory. Symmetry point groups are not identified because structures resulted from a stochastic global search imposing no symmetry.

The lowest energy structures are nearly degenerate octets, of the quasi-C_s and -C_{2v} symmetries. Looking at Figure 2, we see a few motifs repeating throughout the isomer energy spectrum. For example, the same D_{2h} structure is seen in Figure 2 numbers 18, 19, 22, and 26 with two multiplicities and over a range of 1.21 eV. This repetition of nearly identical but not energetically degenerate structures is present for all of the low-lying isomers including the quasi-degenerate global minima.

DOI: 10.1021/acs.jpca.7b00247
J. Phys. Chem. A 2017, 121, 1849−1854

This is indicative of several features of these clusters. First the energy wells by the attached cluster minimum are relatively flat with respect to Sm moving around the B_6 unit. This could imply that the boron−samarium interaction is a weaker bond than other metal−boron coordination. Additionally, it is possible that the small energy differences are an artifact of DFT, and this necessitates considering the lowest minima with *ab initio* methods.

The lowest energy structures are all those with all six boron atoms bonded together, and the number of B−B bonds roughly correlates with the energy of the isomer. For example, the fan-shaped isomer 13 (2.361 eV above the global minimum) is higher in energy than the puckered-fan isomer 10 (1.533 eV above the global minimum). Overall, the results of the geometry optimization are in line with what we might expect from a boron cluster. The energetic stability afforded by all the boron atoms being together is clearly present, and the boron networks look much like solitary gas phase boron clusters.

We will take the DFT optimized geometries, and subject them to higher-level treatment, to winnow out which is the actual global minimum and calculate the photoelectron spectrum.

Taking the C_{2v} and C_s structures from our global optimization, we calculated the vertical electron detachment energy by looking at the difference between the energies of the octet anion and both the nonet and septet neutral. Unfortunately for DFT, the switch from PBE0 to B3LYP and the switch from ZORA to DKH2 both swapped the energetic ordering of the isomers. Additionally, the TD-DFT spectra themselves produced negative excitations and were nearly continuous—a clear sign of linear response methods being qualitatively incorrect. Along with the likely prospect of state trapping, these problems with DFT further motivate our need for *ab initio* methods.

To assess what methods would best describe our clusters, we performed CASSCF(13,16) calculations to determine the multireference character of the two lowest minima. Both anions proved to be intrinsically multireference with the Hartree−Fock solution having a CI coefficient less than 0.6. The large degree of multireference character combined with the large number of electrons in the system informs us that dynamic electron correlation needs to be included, and our method of choice for this system is CASPT2. For the CASPT2 and initial CASSCF calculations, we selected the all-electron cc-pVDZ-DK basis set for B and the cc-pVDZ-DK3 basis set for Sm. We selected a CASSCF(11,13) reference calculation as the starting point for all of our PT2 calculations. To aid in convergence, a level shift of 0.3 was applied to all PT2 calculations. All *ab initio* calculations were performed with Molpro 2015.[24,25]

Because the photoelectron spectrum requires a high degree of accuracy for the relativistic corrections, we need to benchmark the relativistic Douglass−Kroll−Hess (DKH) approximation for this system.[26] While ZORA was sufficient for the geometry optimization, we use DKH for the single point calculations because it offers a tunable accuracy. In the limit of infinite order, the DKH approaches the exact spin-free electron-only Dirac Hamiltonian. In most applications the second order is sufficient to capture the scalar relativistic effects and is considered the standard. We found that at the second order neither the absolute energies of the anion and neutral species nor the energy differences between the two were reliable (Table 1). We needed to go to the sixth-order DKH before the absolute energy of the anion stabilized sufficiently. The energy differences between the neutrals and the anion began to converge by the fourth-order DKH, but we chose to run all our *ab initio* spectrum calculations at the sixth order for added assurance and accuracy. The energy differences reported in Table 1 are not unreasonably large: in the original paper describing the arbitrary order DKH method by Reiher et al., the change in energy between DKH2 and DKH4 for a single gold atom was −370 eV.[27] It must also be noted that the DKH approximation is spin-free; however, spin−orbit coupling should not be an issue for the low-lying excitations in this cluster because the adjacent spin states are far apart in energy.

Table 1. Relative Energy of the C_{2v} Anion with Respect to the DKH2[a]

DKH order	energy (eV)	VDE (eV)
DKH2	0.0	2.53
DKH4	−125.6	1.70
DKH6	−129.4	1.75
DKH8	−129.8	*b*

[a]The second order is entirely insufficient and misses a large amount of the relativistic energy. By the fourth order it has recovered enough of the energy to generate excitations within the 0.1 eV experimental error. [b]No convergence was obtained for DKH8 on the neutrals.

With CASPT2+DKH6, we find that the octet C_{2v} isomer is the lowest energy structure, beating out the octet C_s by a 0.24 eV. We can now solely consider the C_{2v} structure for the purposes of determining the bonding and photoelectron spectrum.

RESULTS AND DISCUSSION

The first VDE (feature X, Figure 1 and Table 2) to the septet was calculated to be 1.75 eV, in agreement with the 1.70 ± 0.1 eV experimentally observed VDE. The corresponding adiabatic detachment energy (ADE) was calculated by PBE0 optimizing the septet, exactly as we did for the global optimization, and then running a CASPT2+DKH6 single point. The calculated ADE (A) of 1.43 eV was also in agreement with experimental ADE of 1.35 ± 0.1 eV. Another feature (B) corresponds to a photodetachment to an excited state septet and is calculated to be 1.85 eV, in agreement with the experimental 1.85 ± 0.1 eV. Past the shoulder, a small peak (C) was shown to be yet another detachment to a final excited septet state. The experimental and the theoretical values, 2.05 ± 0.1 and 1.97 eV, respectively, coincide. Finally, the detachment to a nonet, $^9A_2$ (D), was calculated to be 2.31 eV and corresponds to a not

Table 2. CASPT2+DKH6 Excitation Energies from the Septet Neutral[a]

label	state	calcd energy (eV)	exptl energy (eV)
	$^8B_2$	0.00	0.00
A	$^7B_2$ ADE	1.43	1.35 ± 0.1
X	$^7B_2$ VDE	1.75	1.70 ± 0.1
B	$^7B_2$	1.85	1.85 ± 0.1
C	$^7B_2$	1.97	2.05 ± 0.1
D	$^9A_2$	2.31	2.30 ± 0.1

[a]The spectroscopic states are taken from the Kohn−Sham orbitals and the largest weighted CI coefficient. $^8B_2$ is defined as the ground state. The differences between the experiment and theory are well within the experimental error and the expected variance of DKH6.

DOI: 10.1021/acs.jpca.7b00247
J. Phys. Chem. A 2017, 121, 1849−1854

fully resolved peak in a very populated area of the spectrum. The density of excited states past feature D is such that we cannot assign meaningful transitions to each peak or, in fact, even distinguish them from experimental error or each other. The pile-up of so many excited septet states and nonet states will make the SO coupling nonignorable and intractable. All data past 2.5 eV can be seen as many excitations on top of one another.

As will be shown in the next section, all of the lowest energy spectral features correspond to the photodetachment channels from the B_6 unit in the cluster, as the highest occupied orbitals are centered on boron and involve minimally the contributions from Sm. Considering that (i) the binding of Sm to the boron cluster is weak, (ii) the B_6^- structure in several low-energy isomers of SmB_6^- is preserved, (iii) many isomers are within a small energy range from the global minimum at varying levels of theory, and (iv) the lowest channels in the spectrum correspond to the photodetachment from boron, we are forced to suspect that several isomers of SmB_6^- could produce similar spectra in agreement with the experiment. Thus, in this case, the agreement with the experiment is possibly not fully assuring of the structure. Our C_{2v} structure is produced at the highest level of theory possible today, and the agreement with the experiment is great; yet we opt to leave this structure as a proposal. We are confident to state, however, that the experimentally observed isomer or isomers should contain a connected boron cluster, with the highest occupied MOs belonging to boron.

To understand the bonding in this cluster, we first look at the Kohn–Sham orbitals of the octet anion (Figure 3). In general, the delocalized boron bonding stays intact as it would be found in the B_6^{2-} cluster. This is seen particularly well in the lowest energy orbitals: $1a_1$, $1b_2$, $2a_1$, and $2b_2$ form a sigma bonding and antibonding system, and $3a_1$, $4a_1$, $3b_2$, and $4b_2$ from a peripheral sigma bonding and antibonding system. There is also clearly a π-antiaromatic system composed of $1b_1$ and $1a_2$. By employing a natural population analysis (NPA), we see that the B_6 portion of SmB_6^- caries a −1.796 charge, meaning it is close in electronic structure to the B_6^{2-} cluster. The charge of +0.796 on Sm is approximately the Sm(I) oxidation state. The difference between the −2 anion of B_6 and the +1 cation of Sm is shared between the two units in the form of covalent bonds, which we will further examine.

The higher energy orbitals of SmB_6^- also show delocalized boron bonding, but there the Sm f orbitals and d orbitals have a significant overlap with the delocalized sigma antibonding orbitals. This is somewhat similar to previous reports of metals binding to boron clusters.[28] With LaB_n^- clusters, the d orbitals join into the p orbital networks. Additionally, in TaB_6^- the predicted geometry is the same as SmB_6^-, and it possesses a similar bonding scheme.[29] The similarity in structure between TaB_6^- and SmB_6^- suggests that SmB_n^- ($n > 10$) clusters might form wheels with even higher coordination numbers than Ta. However, both the TaB_6^- and the LaB_n^- clusters are vastly different from the SmB_6^- cluster because no multireference character was necessary to reproduce the spectrum (both papers used the inherently single reference CCSD(T)). The major bonding difference is that here we have f orbitals participating directly in the valence bonding, which is unusual because of their relativistic contraction. Because of the participation of the f and d orbitals in the bonding, it becomes difficult to assess the bonding types present in the remaining

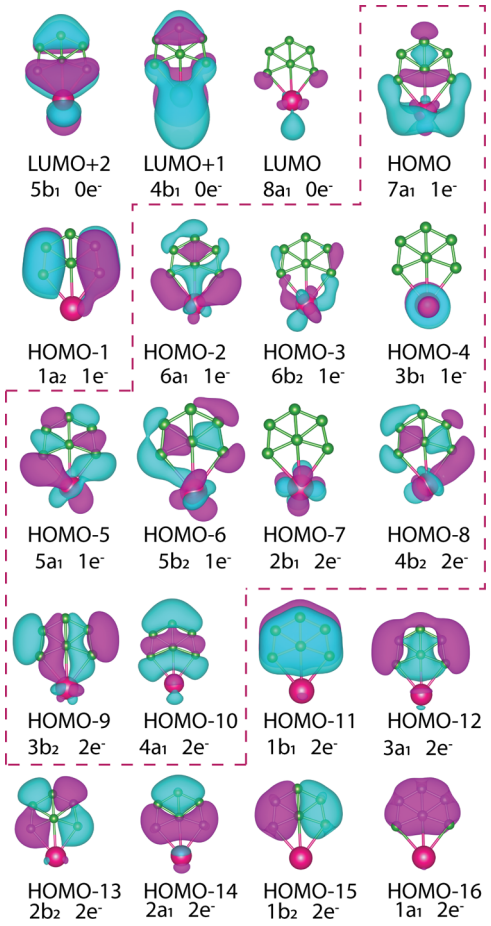

Figure 3. Valence and lowest energy unoccupied Kohn–Sham orbitals of SmB_6^-. Clearly present are the aromatic and delocalized bonding motifs seen in the isolated B_6^- cluster. Interestingly, the f orbitals are shown to have significant overlap with the sigma antibonding systems.

orbitals. For this situation, the adaptive natural density partitioning (AdNDP) analysis is indispensible.[30]

An AdNDP analysis is helpful in determining what types of bonds actually result from the calculated alpha electron density. Using the alpha density means the maximum occupation of our bonds is 1.00. Our AdNDP analysis localized two center–two electron (Lewis) bonds between the perimeter borons (Figure 4), with good occupation numbers of 0.98, 0.98, 0.96, 0.96, 0.82, and 0.82 e^-. It also recovers the delocalized antiaromatic system seen in $1a_2$ and $1b_1$. These are both fully occupied with 1.00 e^- each. By checking this result against the KS orbitals, we note that the delocalized π-system contains a total of three electrons, a pair in the HOMO−11, and a single electron in the HOMO−1, since the system is an octet. Hence, in this situation, the Hückel's electron-counting rule of $4n$ for antiaromatic compounds does not hold up, but the antiaromaticity can nevertheless be claimed. Additionally, AdNDP finds an antiaromatic σ-system from the remaining electron density. This system also has good electron counts of 0.99 and 0.70 e^-. Therefore, we can classify the C_{2v} as doubly antiaromatic, σ and π. Double antiaromaticity was observed also in the B_6^- cluster ion in isolation, although its planar structure is slightly different. In addition to both of the antiaromatic networks, there remains a peripheral Sm–B bond of a_1 symmetry (σ-type). This bond is composed of p orbitals on boron and both f and d orbitals on Sm and has an occupation

DOI: 10.1021/acs.jpca.7b00247
J. Phys. Chem. A 2017, 121, 1849–1854

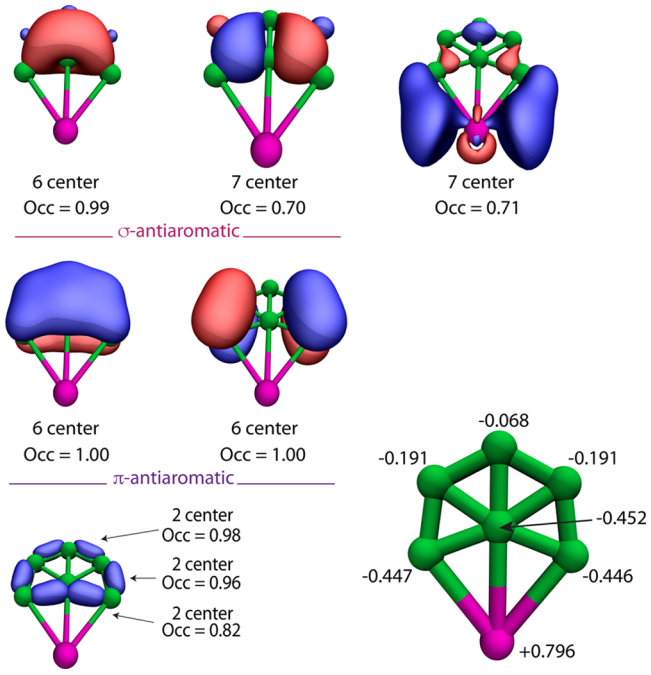

Figure 4. AdNDP analysis for SmB_6^-. The annotated cluster in the bottom right shows the natural population analysis charges. Because this is an AdNDP analysis of the alpha density, a fully occupied orbital has an Occ = 1.00. The lower left bonds are the six 2c−2e bonds joining the peripheral borons. The occupation numbers are the same for each pair of bonds. The middle left two bonds show the π-antiaromatic system. The top two bonds on the left are the σ-antiaromatic system. The top right bond is the peripheral sigma Sm−B bond. Not shown are the 1c−2e bonds that are simply nonbonding core orbitals on each atom.

of 0.71 e^-. The presence of bonding f orbitals, even in a hybrid, is novel, since f orbitals are normally considered too contracted to play any role in valence states. This observation brings f orbitals into the fray. The way Sm binds to the boron cluster is reminiscent of how d-block elements bind to boron, except the latter use d orbitals, whereas Sm heavily involves f orbitals as well.

CONCLUSION

We showed that SmB_6^- is an incredibly sensitive system possessing relativistic effects and electron correlation thoroughly outside the realm of go-to DFT treatments and single reference methods. In order to accurately reproduce the experimental photoelectron spectrum, this system required a *tour de force* of computational chemistry's finest methods: excited state CASPT2 and sixth-order relativistic effects. The only area where we retain confidence in DFT for this system is in predicting the geometries. Far from only being a challenging quantum mechanical puzzle, SmB_6^- also possesses fascinating bonding properties. AdNDP analysis shows that its C_{2v} structure retains the double antiaromaticity of B_6^{2-} and also incorporates f orbitals into a Sm−B covalent bond. This recruitment of f-orbitals into the bonding fray opens up the possibility of designing larger clusters with never-before-seen bonding motifs.

AUTHOR INFORMATION

Corresponding Authors

*E-mail kbowen@jhu.edu (K.H.B.).

*E-mail ana@chem.ucla.edu (A.N.A.).

ORCID

Anastassia N. Alexandrova: 0000-0002-3003-1911

Notes

The authors declare no competing financial interest.

ACKNOWLEDGMENTS

This work was supported by the Air Force Office of Scientific Research (AFOSR) under Grant FA9550-15-1-0259 (K.H.B.), Grant FA9550-16-1-0141 (A.N.A.), NSF Career Award CHE1351968 (A.N.A.), and the generous donation of Ms. Evers-Manly as part of the Undergraduate Research Scholars Program of the UCLA Undergraduate Research Center-Sciences (P.J.R.). UCLA IDRE cluster Hoffman2 was used for all calculations.

REFERENCES

(1) Zhai, H.-J.; Wang, L.-S.; Alexandrova, A. N.; Boldyrev, A. I.; Zakrzewski, V. G. Photoelectron Spectroscopy And Ab Initio Study Of B_3^- And B_4^- Anions And Their Neutrals. *J. Phys. Chem. A* **2003**, *107*, 9319−9328.

(2) Piazza, Z. A.; Hu, H. S.; Li, W. L.; Zhao, Y. F.; Li, J.; Wang, L. S. Planar Hexagonal B(36) As A Potential Basis For Extended Single-Atom Layer Boron Sheets. *Nat. Commun.* **2014**, *5*, 3113.

(3) Zhai, H. J.; Zhao, Y. F.; Li, W. L.; Chen, Q.; Bai, H.; Hu, H. S.; Piazza, Z. A.; Tian, W. J.; Lu, H. G.; Wu, Y. B.; et al. Observation Of An All-Boron Fullerene. *Nat. Chem.* **2014**, *6*, 727−31.

(4) Oger, E.; Crawford, N. R.; Kelting, R.; Weis, P.; Kappes, M. M.; Ahlrichs, R. Boron Cluster Cations: Transition From Planar To Cylindrical Structures. *Angew. Chem., Int. Ed.* **2007**, *46*, 8503−8506.

(5) Wang, L.-S. Photoelectron Spectroscopy Of Size-Selected Boron Clusters: From Planar Structures To Borophenes And Borospherenes. *Int. Rev. Phys. Chem.* **2016**, *35*, 69−142.

(6) Romanescu, C.; Galeev, T. R.; Li, W.-L.; Boldyrev, A. I.; Wang, L.-S. Transition-Metal-Centered Monocyclic Boron Wheel Clusters (M©Bn): A New Class of Aromatic Borometallic Compounds. *Acc. Chem. Res.* **2013**, *46*, 350−358.

(7) Jian, T.; Li, W.-L.; Popov, I. A.; Lopez, G. V.; Chen, X.; Boldyrev, A. I.; Li, J.; Wang, L.-S. Manganese-Centered Tubular Boron Cluster − MnB_{16}^-: A New Class Of Transition-Metal Molecules. *J. Chem. Phys.* **2016**, *144*, 154310.

(8) Popov, I.; Jian, T.; Lopez, G.; Boldyrev, A.; Wang, L. Cobalt-Centred Boron Molecular Drums With The Highest Coordination Number In The CoB_{16}^- Cluster. *Nat. Commun.* **2015**, *6*, 8654.

(9) Alexandrova, A. N.; Boldyrev, A. I.; Zhai, H.-J.; Wang, L.-S. All-Boron Aromatic Clusters As Potential New Inorganic Ligands And Building Blocks In Chemistry. *Coord. Chem. Rev.* **2006**, *250*, 2811−2866.

(10) Alexandrova, A. N.; Boldyrev, A. I.; Zhai, H.-J.; Wang, L.-S.; Steiner, E.; Fowler, P. W. Structure And Bonding In B_6^- And B_6: Planarity And Antiaromaticity. *J. Phys. Chem. A* **2003**, *107*, 1359−1369.

(11) Alexandrova, A. N.; Zhai, H.-J.; Wang, L.-S.; Boldyrev, A. I. Molecular Wheel B_8^{2-}As A New Inorganic Ligand. Photoelectron Spectroscopy And Ab Initio Characterization Of LiB_8. *Inorg. Chem.* **2004**, *43*, 3552−3554.

(12) Cordero, B.; Gómez, V.; Platero-Prats, A. E.; Revés, M.; Echeverría, J.; Cremades, E.; Barragán, F.; Alvarez, S. Covalent Radii Revisited. *J. Chem. Soc., Dalton Trans.* **2008**, 2832−2838.

(13) Dzero, M.; Sun, K.; Galitski, V.; Coleman, P. Topological Kondo Insulators. *Phys. Rev. Lett.* **2010**, *104*, 106408.

(14) Cooley, C.; Aronson, M.; Fisk, Z.; Canfield, P. SmB_6 - Kondo Insulator Or Exotic Metal. *Phys. Rev. Lett.* **1995**, *74*, 1629−1632.

(15) Neupane, M.; Alidoust, N.; Xu, S.; Kondo, T.; Ishida, Y.; Kim, D.-J.; Liu, C.; Belopolski, I.; Jo, Y.; Chang, T.-R. Surface Electronic Structure Of The Topological Kondo-Insulator Candidate Correlated Electron System SmB_6. *Nat. Commun.* **2013**, *4*, 2991.

DOI: 10.1021/acs.jpca.7b00247
J. Phys. Chem. A 2017, 121, 1849−1854

(16) Antonov, V. N.; Shpak, A. P.; Yaresko, A. N. Electronic Structure Of Mixed ValentSystems. *Condens. Matter Phys.* **2004**, *7*, 211−246.
(17) Zhang, X.; Wang, Y.; Wang, H.; Lim, A.; Gantefoer, G.; Bowen, K. H.; Reveles, J. U.; Khanna, S. N. On The Existence Of Designer Magnetic Superatoms. *J. Am. Chem. Soc.* **2013**, *135*, 4856−4861.
(18) Zhang, X.; Robinson, P.; Gantefor, G.; Alexandrova, A.; Bowen, K. Photoelectron Spectroscopic And Theoretical Study Of The $[HPd(h^2\text{-}H_2)]^-$ Cluster Anion. *J. Chem. Phys.* **2015**, *143*, 094307.
(19) Ho, J.; Ervin, K. M.; Lineberger, W. C. Photoelectron Spectroscopy Of Metal Cluster Anions: Cu^-_n, Ag^-_n, And Au^-_n. *J. Chem. Phys.* **1990**, *93*, 6987−7002.
(20) Adamo, C.; Barone, V. Toward Reliable Density Functional Methods Without Adjustable Parameters: The PBE0Model. *J. Chem. Phys.* **1999**, *110*, 6158−6170.
(21) Pantazis, D.; Neese, F. All-Electron Scalar Relativistic Basis Sets for the Lanthanides. *J. Chem. Theory Comput.* **2009**, *5*, 2229−2238.
(22) Francl, M. M.; Pietro, W. J.; Hehre, W. J.; Binkley, J. S.; Gordon, M. S.; DeFrees, D. J.; Pople, J. A. Self-Consistent Molecular Orbital Methods. XXIII. A Polarization-Type Basis Set For Second-Row Elements. *J. Chem. Phys.* **1982**, *77*, 3654−3665.
(23) Valiev, M.; Bylaska, E.; Govind, N.; Kowalski, K.; Straatsma, T.; Van Dam, H.; Wang, D.; Nieplocha, J.; Apra, E.; Windus, T.; et al. NWchem: A Comprehensive And Scalable Open-Source Solution For Large Scale Molecular Simulations. *Comput. Phys. Commun.* **2010**, *181*, 1477−1489.
(24) Celani, P.; Werner, H.-J. Multireference Perturbation Theory For Large Restricted And Selected Active Space Reference Wave Functions. *J. Chem. Phys.* **2000**, *112*, 5546−5557.
(25) Werner, H.-J.; Knowles, P. J.; Knizia, G.; Manby, F. R.; Schütz, M. Molpro: A General-Purpose Quantum Chemistry Program Package. *Wiley. Interdiscip. Rev. Comput. Mol. Sci.* **2012**, *2*, 242−253.
(26) Liu, W.; Peng, D. Infinite-Order Quasirelativistic Density Functional Method Based On The Exact Matrix Quasirelativistic Theory. *J. Chem. Phys.* **2006**, *125*, 044102.
(27) Reiher, M.; Wolf, A. Exact Decoupling Of The Dirac Hamiltonian. II. The Generalized Douglas−Kroll−Hess Transformation Up To Arbitrary Order. *J. Chem. Phys.* **2004**, *121*, 10945−10956.
(28) Cheng, S.-B.; Berkdemir, C.; Castleman, A. Observation Of d−p Hybridized Aromaticity In Lanthanum-Doped Boron Clusters. *Phys. Chem. Chem. Phys.* **2014**, *16*, 533−539.
(29) Li, W.-L.; Ivanov, A. S.; Federič, J.; Romanescu, C.; Černušák, I.; Boldyrev, A. I.; Wang, L.-S. On The Way To The Highest Coordination Number In The Planar Metal-Centred Aromatic Ta©B10− Cluster: Evolution Of The Structures Of TaB_n^- (N= 3−8). *J. Chem. Phys.* **2013**, *139*, 104312.
(30) Zubarev, D. Y.; Boldyrev, A. I. Developing Paradigms Of Chemical Bonding: Adaptive Natural Density Partitioning. *Phys. Chem. Chem. Phys.* **2008**, *10*, 5207−5217.

DOI: 10.1021/acs.jpca.7b00247
J. Phys. Chem. A 2017, 121, 1849−1854